Experimental Tests on Fillet and PJP Welds in CHS Moment T-Connections

Zhiyuan Yang[a] and Kyle Tousignant[a*]

[a] Department of Civil Engineering, Dalhousie University, 1360 Barrington Steet, P.O. Box 15000, Halifax NS, B3H 4R2, Canada

[*] Corresponding Author. E-mail: kyle.tousignant@dal.ca; Tel: +1-902-494-3180

Abstract

An experimental program was developed at Dalhousie University to test various unreinforced circular hollow section (CHS)-to-CHS 90° T-connections subjected to branch in-plane bending moment with the objective of determining the effective section properties of the welded joints. Eleven specimens were designed to be weld-critical (i.e., to fail by weld rupture), and tested by applying a single quasi-static point load, laterally, to the top of each branch. An equation for the weld effective section modulus for CHS-to-CHS moment T-connections is developed, and various design formulae are assessed through a first-order reliability method analysis. The scope of this research covers fillet and partial-joint-penetration groove welded connections with $0.31 \leq$ branch-to-chord width ratio ≤ 0.91, $31 \leq$ chord wall slenderness ≤ 46, and $0.75 \leq$ branch-to-chord thickness ratio ≤ 1.00. Recommendations are made for weld design using the "effective length approach" in AISC 360.

Key words

Hollow structural sections, circular hollow sections, fillet welds, groove welds, effective lengths, effective lengths, connections, experiments

1. Introduction

Various international codes, standards, and design guides [1-5] acknowledge two different sizing philosophies for welds between hollow structural sections (HSS):

1. The weld can be sized to develop the yield strength of the connected branch. Using the yield strength of branch as the design strength of a welded joint produces an upper bound on the weld size.

2. The weld can be sized as “fit for purpose”, to resist the actual force(s) in the connected branch. This method requires the use of “weld effective properties” (lengths or section moduli) for the weld group – to take into account the nonuniform load transfer that occurs through the weld around an HSS branch perimeter [6-20].

Method 1 is generally appropriate when the design force(s) in the branch, or the use of Method 2, are uncertain, or when plastic stress redistribution is required in the connection. Method 2, on the other hand, can result in smaller weld sizes (particularly for lightly loaded branches), which can increase connection efficiency, and lower fabrication cost.

Over the last 30 years, weld-critical tests (i.e., tests that are designed to fail by weld fracture) have been used to study the strength and behaviour of welds in rectangular hollow section (RHS) connections [6-10]. These tests, and subsequent recommendations, have led to the widespread acceptance of Method 2 (i.e., designing welds as fit-for-purpose) for RHS connections, and the development of Table K5.1 (formerly, Table K4.1) – “Effective Weld Properties for Connections to Rectangular HSS” in AISC 360-16 [4], based on this approach.

In recent years, similar recommendations have been made for weld effective *lengths* in axially loaded circular hollow section (CHS) connections. These recommendations (for CHS T-, Y-, and X-connections) have been evaluated for use in conjunction with AISC 360 [4], CSA S16:19 [5], and Eurocode by Tousignant and Packer [13; 15-19] and were recently introduced into the forthcoming edition of AISC 360 (AISC 360-22) as Table K5.2 – “Effective Weld Properties for Connections to Round HSS” [23].

While Table K5.2 provides a necessary step towards the widespread adoption of Method 2 for welds in CHS connections, a considerable amount of work is still needed for its development, so that – as a long-term goal – it can match Table K5.1 in its coverage of both connection types (e.g., K- and N-connections) and loadings (e.g., in-plane bending, out-of-plane bending).

To this end, an experimental program was developed at Dalhousie University to test various unreinforced CHS-to-CHS moment T-connections – to investigate the flexural strength of the weld(s) around the CHS branch(es) under in-plane bending. Hence, a total of 11 90° CHS-to-CHS moment T-connections were designed and fabricated with variations in weld type (fillet or partial-joint penetration), branch-to-chord width ratio (β) (ranging from 0.31 to 0.91), chord wall slenderness (D/t) (of 31, 34, 35, 38 and 46), and branch-to-chord thickness ratio (τ) (ranging from 0.75 to 1.00).

In this paper, the experimental program is described, in detail, the results are presented, and various weld design formulae are assessed using a first-order reliability method (FORM) analysis. Calculated ranges of the reliability index (β^+) obtained from the FORM approach are compared to the β^+ values obtained using the so-called "expanded separation factor" (ESF) approach [21,22], and to AISC's target value of $\beta^+ = 4.0$ for connectors per Chapter B of the AISC 360-16 Commentary [4]. Recommendations are made for the "fit-for-purpose" design of welds in CHS-to-CHS moment T-connections that are suitable for adoption into the new AISC 360 Table K5.2 [23].

2. Experimental Program

2.1. Test Specimen Design

Eleven directly welded CHS-to-CHS moment T-connections were designed to be weld-critical. The specimens were designed (and fabricated) from ASTM A500 Grade C cold-formed CHS [24] (with a nominal yield strength of $F_y = 317$ MPa). Their geometric configurations were selected based on available materials from the supplier (Atlas Tube Inc.) and to cover a range of key parameters that influence connection (and weld) strength. The experimental test designations (Specimen ID), measured HSS dimensions, and key parameters (i.e., β, D/t, and τ) are summarized in Table 1. As shown in Table 1, all HSS members of the same size were from the same heat (and had the same measured dimensions) which, when arranged for the test specimens, resulted in values of $0.31 \leq \beta \leq 0.91$, $31 \leq D/t \leq 46$, $0.70 \leq \tau \leq 1.00$, and branch inclination angle(s) of $\theta = 90°$. The value of α in Table 1 [i.e., the nondimensional chord length parameter ($\alpha = 2l/D$, where l and D are as shown in Fig. 1)], was selected based on the work of Van der Vegte and Makino [25] and Tousignant [26] to avoid end effects on the connection. To economize on material, both the branches and the chords of all connections were left uncapped at the ends. The layout for the specimens described herein is shown in Fig. 1. Typical weld details are shown in Fig. 2.

Table 1. Test specimen details and key parameters (*two-column table*)

Specimen ID	HSS Dimensions		β^{a}	D/t	τ	α	θ (°)	Connection Failure Mode [b]	Connection Strength (kNm)
	Branch	Chord							
T324-127-1F	127.6 × 8.9	325.0 × 9.3	0.39	34.9	0.95	13.96	90	CW	32.20
T356-127-1F	127.6 × 8.9	355.9 × 9.3	0.36	38.2	0.95	15.28	90	CW	30.76
T406-127-1F	127.6 × 8.9	407.4 × 8.9	0.31	45.8	0.99	18.31	90	SY	27.56
T406-127-0.7F	127.6 × 8.9	407.4 × 11.8	0.31	34.5	0.75	13.79	90	CW	40.12
T273-127-1P	127.6 × 8.9	274.0 × 8.9	0.47	30.9	1.00	12.38	90	CW	31.72
T356-273-1P	274.0 × 8.9	355.9 × 9.3	0.77	38.2	0.95	15.28	90	CW	142.06
T356-324-1P	325.0 × 9.3	355.9 × 9.3	0.91	38.2	1.00	15.28	90	CW	199.84
T406-273-1P	274.0 × 8.9	407.4 × 8.9	0.67	45.8	1.00	18.31	90	SY	144.87
T406-324-1P	325.0 × 9.3	407.4 × 8.9	0.80	45.8	1.05	18.31	90	SY	178.77
T406-273-0.7P	274.0 × 8.9	407.4 × 11.8	0.67	34.5	0.75	13.79	90	CW	185.25
T406-324-0.7P	325.0 × 9.3	407.4 × 11.8	0.80	34.5	0.79	13.79	90	CW	260.60

[a] Specimens with $\beta < 0.47$ are fillet welded (F-series) connections; test specimens with $\beta \geq 0.47$ are partial joint penetration (PJP) groove-welded (P-series) connections.

[b] SY – shear yielding (calculated in accordance with AISC 360-16 Eq. K4-2); CW – chord wall plastification (calculated in accordance with AISC 360-16 Eq. K4-1) (see Table 2 for HSS material properties).

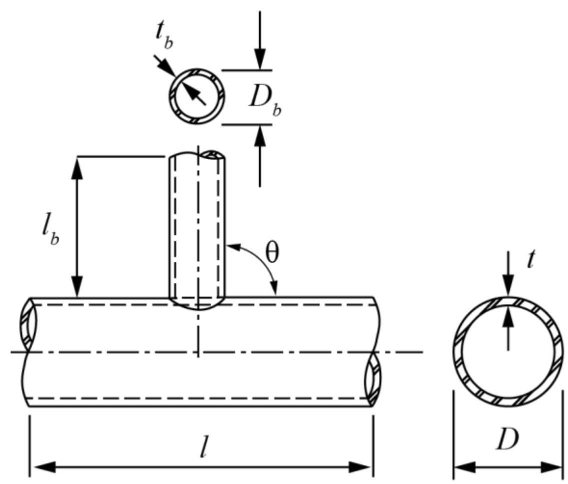

Fig. 1. Test specimen layout and connection nomenclature (one-*column figure*)

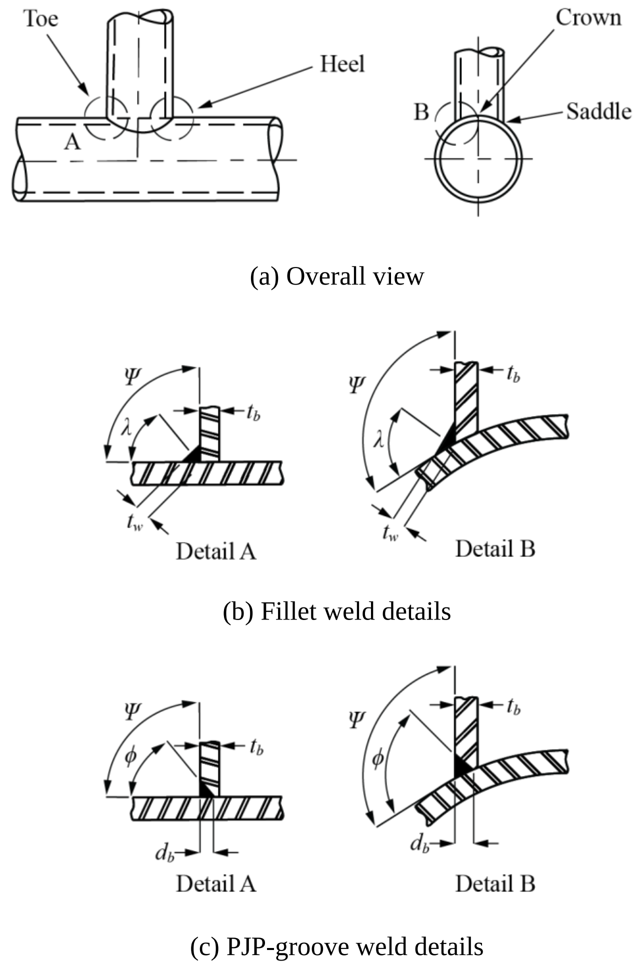

(a) Overall view

(b) Fillet weld details

(c) PJP-groove weld details

Fig. 2. Weld details and joint nomenclature (one-*column figure*)

Connections with $\beta < 0.47$ (the first four, in Table 1) were fillet welded at the branch-to-chord interface (herein termed "F-series"), and connections with $\beta \geq 0.47$ (the next seven, in Table 1) were PJP-groove welded at the interface ("P-series"). This distinction, based on β, was made to ensure sound root penetration in the F-series connections (i.e., no "Z-loss" according to AWS D1.1-20 [27]) by maintaining the local dihedral angle (Ψ) (i.e., the angle between fusion faces on the branch and chord) around the joint (which is a function of β and θ) between 60° and 120°. Detailed discussions on this topic are given by [28]. Herein, it is important to distinguish between both the F-series and P-series connections, as well as the various parameters (β, D/t, and τ).

Nonetheless, all welds were designed to ensure that weld rupture preceded connection failure, whereby the predicted nominal in-plane flexural strength of the weld ($M_{n\text{-}ip}$) (based on conservative assumptions) was less than the corresponding connection strength (for the applicable limit states in Table 1) based on measured CHS properties.

2.2. Test Specimen Fabrication

Branches for the F-series connections were cut to a minimum branch length (l_b) of $6D_b$ to avoid shear lag effects and profiled to saddle perfectly onto the chords without edge bevelling (Fig. 3a). For the P-series connections, the branches were profiled, then bevelled (Fig. 3b), to produce included joint angles of $\phi \geq 60°$ (see Fig. 1b) along the entire weld to avoid Z-loss [27]. The depth of the bevel (d_b, in Fig. 2c) was 6mm (measured perpendicular to the branch) for all tests. To ensure proper fit-up, a computer-numerically controlled (CNC) cutting machine was used to profile and bevel the branches.

(a) T324-127-1F (b) T356-324-1-P

Fig. 3. Fit-up of branch to chord after profiling and bevelling (two-*column figure*)

Prior to welding the tests specimens, trial connections (comprised of a portion of each branch and chord) were cut and checked for fit-up. In addition to ensuring fit-up, these specimens were used to calibrate the welding process parameters to achieve the desired weld size, profile, fusion with the base metal, and root penetration. The final welding process parameters are discussed in Section 3.2. All specimens [i.e., the trial connections, large-scale connections, and all-weld metal tensile coupons (TCs)] were welded using a semi-automatic gas metal arc welding (GMAW) process, with 14mm diameter solid wire(s) (AWS A5.20 E71T) and full CO_2 shielding gas. Welding was performed at a structural fabrication shop (Cherubini Metal Works, in Dartmouth, Nova Scotia) by a qualified welder in the flat and horizontal positions. Photos of the as-laid welds for typical F- and P-series connections are shown in Fig. 4.

(a) T324-127-1-F (b) T406-273-1-P

Fig. 4. As-laid welds, before griding (*two-column figure*)

2.3. Welding and Weld Preparation

The test welds were laid/fabricated to the minimum size requirements of Tables J2.3 and J2.4 of AISC 360-22 for fillet and PJP-groove welds, respectively; however, to ensure weld-critical behaviour, the so-called "as-laid welds" were subsequently ground down to weld sizes that, at the time of testing, were below AISC's minimum values. It is noteworthy that the rationale for Tables J2.3 and J2.4 is to ensure adequate heat input during welding, which was already achieved.

Welds in F-series connections were ground into triangular cross-sections, with flat legs, faces and near-uniform throat sizes (t_w) for each joint. This allowed for t_w to be initially obtained (pre-testing) from external measurements and a 3D model of the exact weld geometry (see Section 3.2.1). The pre-testing measurements were later verified by using macro-etch examinations (see Section 3.2.2).

ASW D1.1 [27] defines the effective throat (t_w) of a fillet weld in a T- and skewed T-joints with $\Psi \geq 60°$ (and, hence, for the CHS-to-CHS moment T-connections in this study) as "the shortest distance from the joint root to the weld face". It is also important to note that the orientation of t_w and the weld legs (l_v and l_h) must be established correctly in the plane of Ψ (which is perpendicular to the weld root, between tangents to the outside surfaces of the branch and the chord).

Welds in P-series connections were ground down into less-precise cross-sectional shapes (see Fig. 3), but with regular-enough geometry to facilitate the accurate measurement of t_w (which is simpler for PJP-groove welded joints compared to fillet-welded joints). It is worth noting here that the throat (t_w) of a PJP groove weld is similarly defined, by AWS D1.1 [27], as "the shortest distance from the root to the face of the diagrammatic weld".

3. Mechanical and Geometrical Properties

3.1. Mechanical and Geometrical properties of the CHS

Mechanical properties of the CHS were determined from TC tests performed in accordance with ASTM A370 [11]. Three TCs were made for each CHS from a one-metre off-cut of the member used in the test program, at 90°, 180°, and 270° from the weld seam. The TCs were tested while maintaining their original curved geometry. Table 2 gives the average measured yield stress (F_y), yield strain (ε_y), ultimate tensile strength (F_u), ultimate strain (ε_u), and Young's Modulus (E) for each section. The yield strength (F_y, in Table 2) was determined by using the 0.2% strain-offset method. The geometrical properties of the CHS (in Table 2, shown previously) were obtained in accordance with methods outlined by the Steel Tube Institute [29].

Table 2. CHS tensile coupon test results (*two-column table*)

Specimen ID	HSS Dimensions		Branch Properties				Chord Properties			
	Branch	Chord	F_y (MPa)	E (GPa)	F_u (MPa)	ε_y (%)	F_y (MPa)	E (GPa)	F_u (MPa)	ε_y (%)
T324-127-1F	127.6 × 8.9	325.0 × 9.3	382	196	494	0.426	417	170	480	0.458
T356-127-1F	127.6 × 8.9	355.9 × 9.3	398	196	466	0.405	417	170	480	0.458
T406-127-1F	127.6 × 8.9	407.4 × 8.9	373	179	483	0.407	417	170	480	0.458
T406-127-0.7F	127.6 × 8.9	407.4 × 11.8	312	211	450	0.350	417	170	480	0.458
T273-127-1P	127.6 × 8.9	274.0 × 8.9	352	198	477	0.205	417	170	480	0.458
T356-273-1P	274.0 × 8.9	355.9 × 9.3	398	196	466	0.405	352	198	477	0.205
T356-324-1P	325.0 × 9.3	355.9 × 9.3	398	196	466	0.405	382	196	494	0.426
T406-273-1P	274.0 × 8.9	407.4 × 8.9	373	179	483	0.407	352	198	477	0.205
T406-324-1P	325.0 × 9.3	407.4 × 8.9	373	179	483	0.407	382	196	494	0.426
T406-273-0.7P	274.0 × 8.9	407.4 × 11.8	312	211	450	0.350	352	198	477	0.205
T406-324-0.7P	325.0 × 9.3	407.4 × 11.8	312	211	450	0.350	382	196	494	0.426

3.2. Mechanical and Geometrical Properties of the Welds

Mechanical properties of the welds were obtained from all-weld-metal TCs created in accordance with Clause 4 of ANSI/AWS D1.1 [27], by welding 25mm-thick steel plates with the dimensions shown in Fig. 5. The TC test specimen was welded using the same electrode spool(s) (same heat no.), equipment, and fabrication processes as both the trial specimens and the F-/P-series connections. The following welding process parameters were used:

- Arc voltage = 26V.
- Wire feed speed = 345ipm.

The all-weld-metal TCs (three total) were saw-cut and machined from the steel test plates at Dalhousie University and fabricated to the general dimensions in Fig. 5. The final dimensions of the reduced section were measured using a calliper and used – in conjunction with a 50-mm extensometer and universal testing machine – to determine F_y, E, electrode ultimate strength (F_{EXX}), and rupture strain (ε_{rup}) (Table 3). As shown in Table 3, the average value of F_{EXX} was 592 MPa.

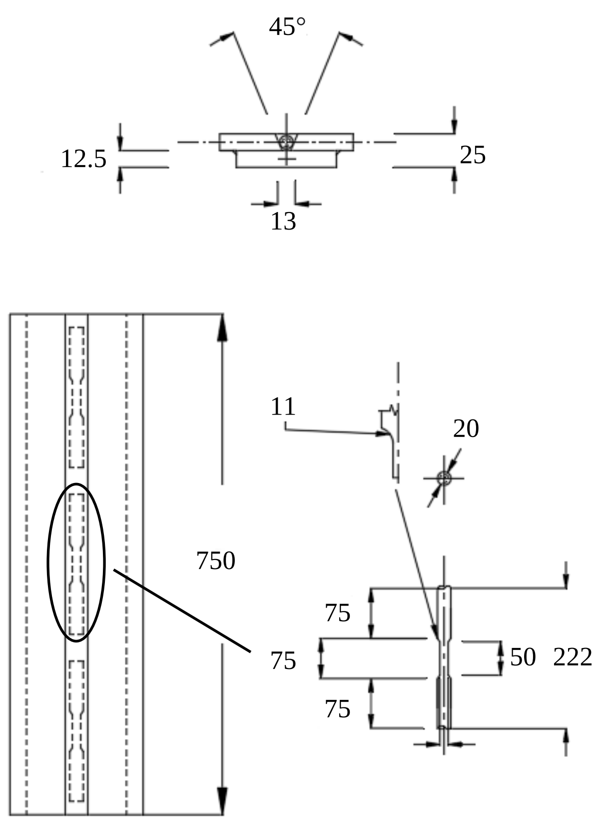

Fig. 5. All-weld-metal tensile coupons (dimensions in mm) (*one-column figure*)

Table 3. All-weld-metal tensile coupon test results (*one-column table*)

Coupon ID	F_y (MPa)	E (MPa)	F_{EXX} (MPa)	ε_{rup} [a] (%)
[i]	560	205000	589	27.9
[ii]	565	216000	593	26.8
[iii]	573	203000	594	26.5
Average	566	208000	592	27.1

[a] Rupture strain determined by re-joining the fractured coupon and measuring: change in gauge length / initial gauge length

3.2.1. Pre-Testing Weld Size Measurements

For the F-series connections, flat weld faces obtained from grinding (see Section 2.3) allowed t_w to be obtained from a 3D model of the weld's "exact" geometry (Fig. 6). First, local components of l_v and l_h in a plane containing the branch axis and the normal to the branch face were measured at 30° increments (12 total locations) along the weld length. The local components of l_v parallel to the branch, and l_h perpendicular to the surface of the branch (Fig. 6a), at each location, were obtained in the manner described by Tousignant and Packer [13]. Using these dimensions, and measured values of D_b and D (Table 1), the weld profile was then modelled in 3D in Solidworks (Fig. 6b). Finally, sections were taken through the weld profile in the true throat-plane orientation (i.e., the plane of Ψ) at each of the 12 measurement locations, from which l_v, l_h and t_w were measured. The average pre-testing "external measurements" of t_w for the F-series connections are summarized in the second column of Table 4. For the F-series connections, the average coefficient of variation (COV) of the 12 throat dimension measurements in each connection was 0.129.

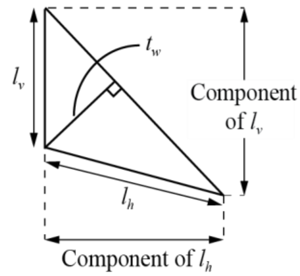

(a) Local components of l_v and l_h

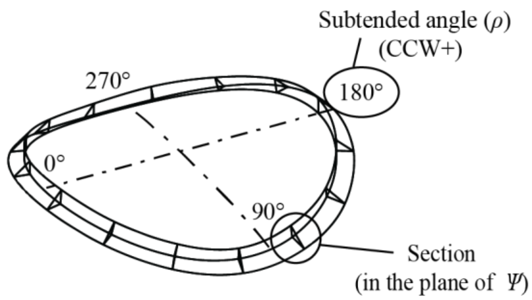

(b) 3D weld profile

Fig. 6. Fillet weld dimensions (*one-column figure*)

Table 4. Pre-testing and post-rupture average weld effective weld throat (t_w) dimension (*two-column table*)

Test Designation	Pre-Testing (mm)	Post-Rupture (mm)		
		MT	FL	CT
T324-127-1F	2.86	2.96	2.97	3.44
T356-127-1F	2.77	2.32	2.33	3.33
T406-127-1F	2.72	2.81	2.90	3.34
T406-127-0.7F	2.65	2.24	2.51	2.91
T273-127-1P	2.98	4.58	4.67	-
T356-273-1P	3.01	5.57	-	-
T356-324-1P	3.83	5.06	5.12	-
T406-273-1P	2.98	4.42	4.42	-
T406-324-1P	3.29	4.11	4.15	-
T406-273-0.7P	2.88	4.95	4.95	-
T406-324-0.7P	3.29	5.36	5.35	-

Note: "-" indicates no data available, or measurement type does not apply for the connection.

For P-series tests, the throat dimension (t_w) after grinding was measured according to Eq. (1):

$$t_w = d_b - d \quad (1)$$

where d = greatest perpendicular dimension measured from a line flush to the branch surface to the weld surface.

As discussed in Section 2.2, d_b is the depth of bevel equal to 6mm. Eq. (1) is valid because the weld details in Fig.

2 ensured full depth of fusion (i.e., no Z-loss). The primary purpose of the pre-test measurements was to ensure: (i) weld-critical behaviour, and (ii) that there was a near-uniform weld throat around the entire joint perimeter. The average pre-testing "external measurements" of t_w for the F-series connections are again summarized in the second column of Table 4. The average COV of the 12 throat dimension measurements for these connections (P-series) was 0.106.

3.2.2. Post-Rupture Weld Size Measurements

After testing, the geometric properties of the test welds were re-measured using macro-etch specimens (Fig. 7). Eight cross sections of the weld profile (two each at subtended angles of ρ = 0°, 90°, 180°, and 270°, as shown in Fig. 6b) were cut, in the plane of Ψ, hand polished, and macro-etched using a 5% nital etchant solution, then digitized at a scale of 1:1 and measured in AutoCAD.

Since, after cutting, each location (i.e., ρ = 0°, 90°, 180°, and 270°) yielded two cross-sections (one on each side), the dimensions l_v, l_h, and t_w were determined by taking the average of eight total measurements per specimen. For each specimen, the weld throat (t_w) determined three ways and compared; i.e:

1. t_w was taken as the minimum distance from the root to the face of the weld (for both F- and P-series tests) in accordance with AWS D1.1 [27] [herein termed the "minimum throat (MT) dimension"];

2. t_w was taken as the distance measured along the weld fracture plane [herein termed the "fracture length (FL) dimension"] (which did not always coincide with the theoretical throat) (see Fig. 7), for comparison; and

3. for F-series tests only, t_w was calculated based on the leg-size measurements (l_v and l_h) and Ψ [herein termed the "calculated throat (CT) dimension"].

The average results for t_w are summarized (previously) in Table 4, and varied within approximately the same range as the external (pre-testing) weld size measurements.

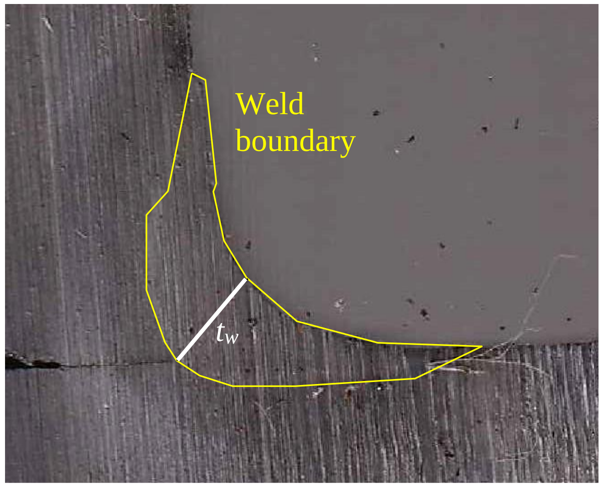

(a) T406-127-1F

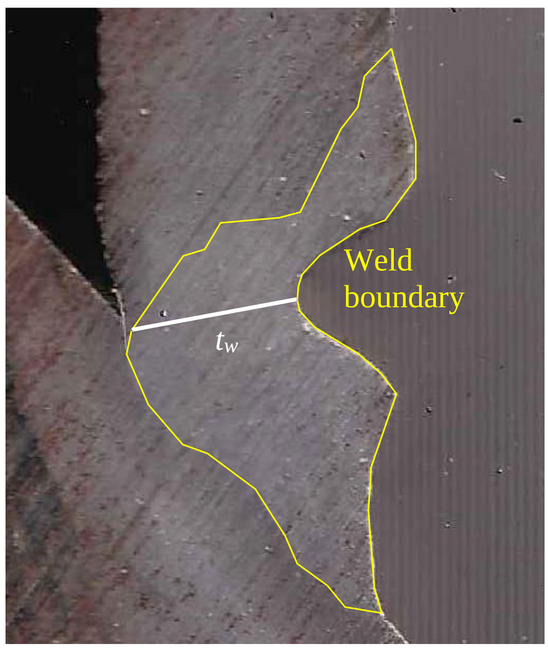

(b) T406-324-1P

Fig. 7. Sample weld cross-sections (MT dimension shown) (*one-column figure*)

By comparing the pre-testing and post-rupture t_w dimensions in Table 4, it is clear that that there is some disparity in the results for the P-series connections. (For the F-series tests, there is actually quite good agreement). In both cases, precedence was given to the post-rupture t_w measurements, which were deemed to be the most reliable.

With respect to the post-rupture t_w measurements, in both cases (i.e., F-series and P-series tests), the MT and FL measurements were similar; hence, while the fracture plane did not always correspond with the weld effective throat plane, the resulting difference in t_w was minimal. In the following analysis (and, generally, in design), the MT measurements have been adopted.

4. Full-Scale Tests

4.1. Test Set-Up and Instrumentation

The test setup assembly for the 11 CHS-to-CHS moment T-connections is shown in Fig. 8. The chord member (i.e., horizontal CHS member) was simply supported at its ends, and the branch member (i.e., the vertical CHS member) was loaded (i.e., pushed on) by a recently calibrated actuator, with a capacity of 500kN and a total stroke of 500mm, to induce an in-plane bending moment in the connection/weld. The test setup was designed to eliminate compressive stress due to axial load in the chord to mitigate chord stress effects.

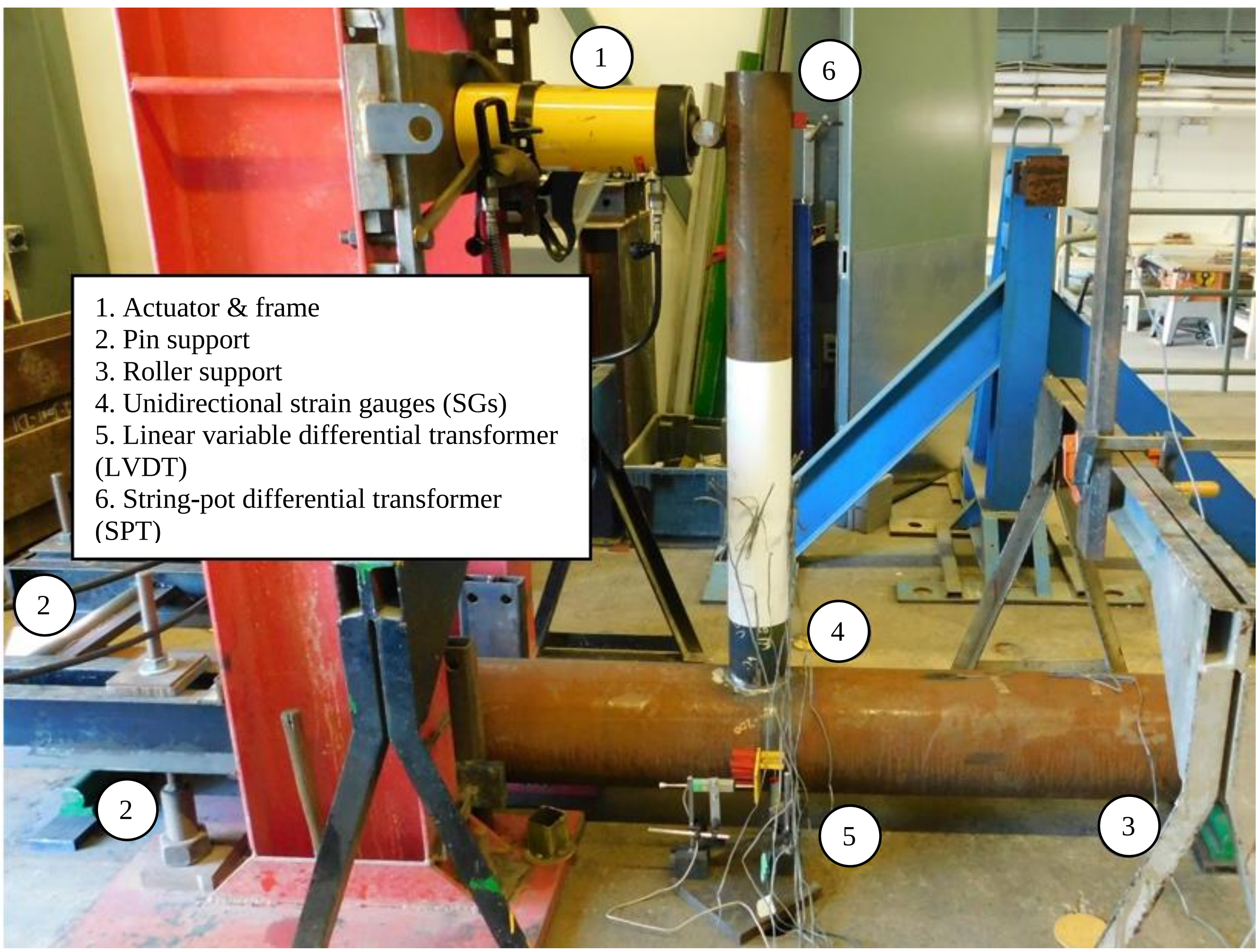

Fig. 8. Elevation of the general test set up assembly for full-scale experiments (*two-column figure*)

Unidirectional strain gauges (SGs) oriented along the longitudinal axis of the branch were installed at eight locations around the branch perimeter, adjacent to the weld, to measure the nonuniform distribution of load transfer through the weld. The SGs (seven of eight) were evenly spaced from the heel (ρ = 0°) to the toe (ρ = 90°), and one additional SG was installed at the saddle point (ρ = 270°, or the theoretical neutral axis) on the opposite side of the branch to monitor for out-of-plane effects. The SGs were placed 15 mm above the weld toe, for both F- and P-series tests, to avoid detecting the high strains that exists close to the weld due to the notch effect [30]. The typical layout of SGs adjacent to the weld is shown Fig 9.

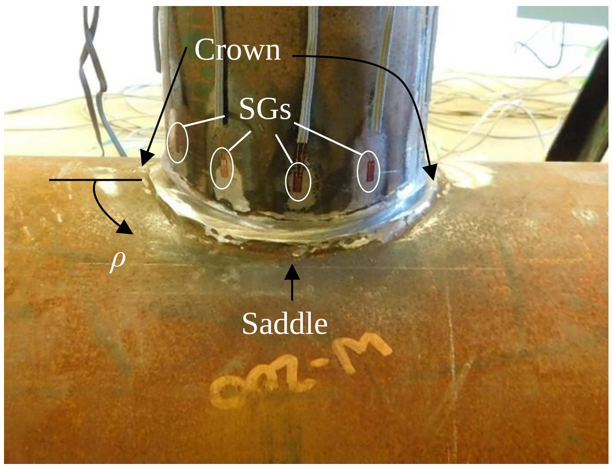

Fig. 9. Typical strain-gauge layout (*one-column figure*)

To determine the branch deflection and chord wall indentation throughout testing, the horizontal displacement at the top of the branch and at the connection work point (i.e., the intersection of the branch and chord centrelines) were measured. The total deflection of the top of the branch relative to the work point (Δ_{total}) was hence determined. The rigid-body deflection (Δ_{rigid}, due to connection rotation) was then inferred by subtracting deflection due to flexure ($\Delta_{flexure} = Pl_b^3/3EI_b$, where I_b = moment of inertia of branch, based on measured dimensions) from Δ_{total}. The branch indentation (Δ_D) into the chord, at the crown, on the compression side, was then calculated from the geometrical relationship in Eq. (2):

$$\Delta_D = \frac{\Delta_{rigid} D_b}{2l_b} \tag{2}$$

5. Results

5.1. Failure Mode, Ultimate Loads and Deformations

All 11 connections failed by weld fracture which initiated near the heel of the connection (at location of the maximum tensile stress) under in-plane bending. Several typical weld failures are shown in Fig. 10.

(a) T406-274-1P

(b) T324-127-1F

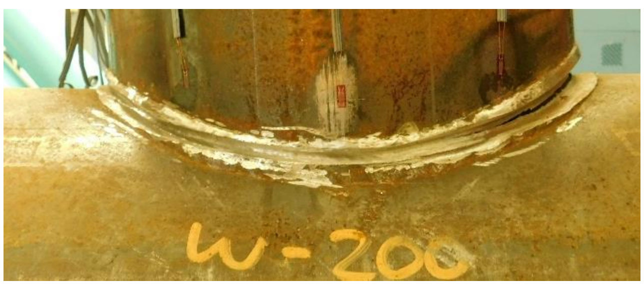

(c) T406-274-1P

(d) T324-127-1F

Fig. 10. Typical weld fractures (*two-column figure*)

In all tests (F- and P-series), the weld failed suddenly along a bumpy plane as expected due to the non-homogeneity of the material and small variations in t_w (due, in part, to non-uniform root penetration). At failure (i.e., at weld fracture), a loud noise (caused by the release of energy) could be heard, and actuator load reading suddenly dropped.

The results, including the applied load (P_a) and moment (M_a) at failure, Δ_{total}, and Δ_D, are summarized in Table 5. It is worth stating that the applied moment at failure (M_a) in Table 5 was calculated at the chord face (i.e., the crown) by multiplying P_a by the lever arm l_b (Fig. 1).

Table 5. Specimen capacity and deformation (*two-column table*)

Test	l_b (to crown) (m)	P_a (kN)	M_a [1] (kNm)	Δ_{total} (mm)	Δ_{rigid} (mm)	$\Delta_{flexure}$ (mm)	Δ_D [2] (mm)	Δ_D/D (%)
T324-127-1F	1.07	34.08	36.47	76.04	61.47	14.57	3.67	1.13
T356-127-1F	1.04	27.28	28.33	42.14	31.47	10.67	1.93	0.54
T406-127-1F	1.02	28.32	28.74	74.18	63.84	10.34	3.99	0.98
T406-127-0.7F	1.02	30.97	31.59	43.33	31.86	11.47	1.98	0.49
T273-127-1P	1.14	34.89	39.77	168.99	150.94	18.04	8.45	3.08
T356-273-1P	1.05	148.46	155.88	91.76	87.13	4.64	11.37	3.19
T356-324-1P	1.04	192.15	199.83	38.69	35.23	3.47	5.50	1.55
T406-273-1P	1.02	127.42	129.97	81.61	77.97	3.65	10.47	2.57
T406-324-1P	1.01	187.10	188.97	48.47	81.37	3.09	13.09	3.21
T406-273-0.7P	1.01	143.54	144.97	33.61	29.62	3.99	10.77	2.64
T406-324-0.7P	1.01	249.11	251.6	71.08	66.97	4.12	4.02	0.99

[1] $M_a = P_a \times l_b$ (to crown).
[2] Eq. (2).

Fig. 11 shows typical plots of applied moment vs. chord indentation (Δ_D) as a % of the chord diameter (D). The vertical line at Δ_D/D = 3% is the widely accepted “chord-plastination limit”. From Fig. 11 (and by comparison of the M_a values for in Tables 5 to the connection strengths in Table 1), three (of the 11) tests exceed the theoretical 3% deformation limit for the chord plastification (CW) limit state. Nevertheless, in all cases, weld fracture was ultimately obtained, and the connections can hence be deemed weld-critical.

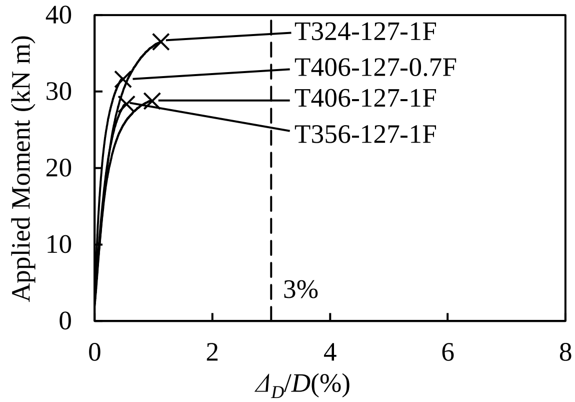

(a) F-series connections

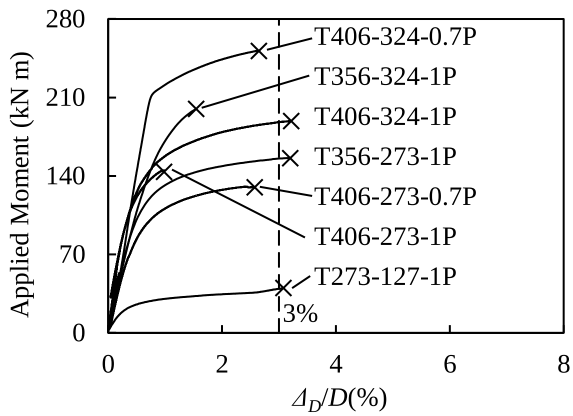

(b) P-series connections

Fig. 11. Applied moment versus chord indentation plots (*one-column figure*)

5.2. Strain Distributions

The stain distribution(s) around the branch adjacent to the weld under the in-plane bending load from several tests are shown in Fig. 12 for varying levels of applied bending moment (at 0.25-, 0.50-, 0.75- and 0.90-times M_a). Fig. 12 shows that even under low (elastic) loads the maximum strain is not located at the extreme bending fibre. This insinuates the presence of a “weld effective length” phenomenon. This phenomenon, and corresponding design provisions in AISC 360 [4], are discussed further in the following section.

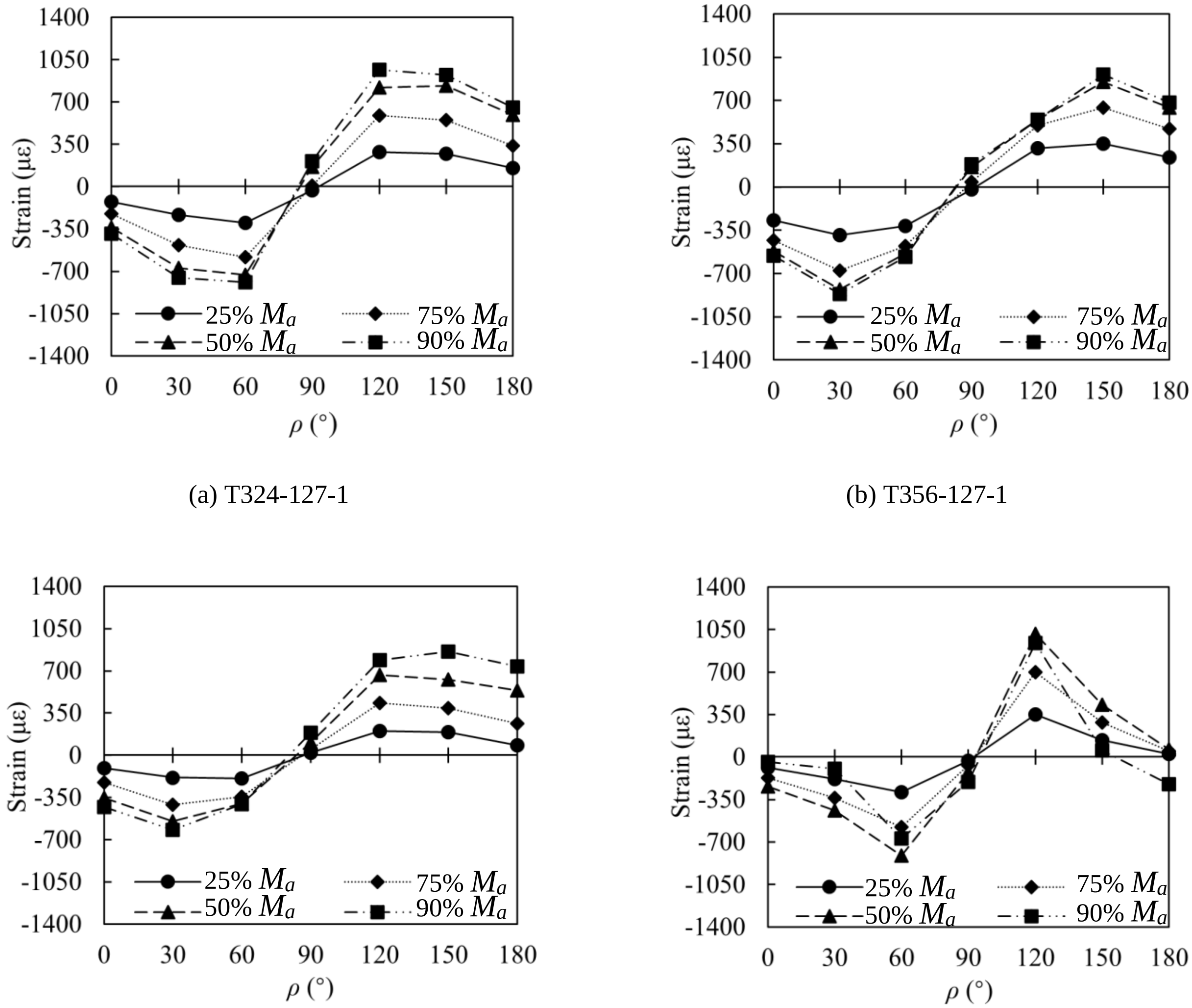

(a) T324-127-1

(b) T356-127-1

(c) T406-127-0.7

(d) T406-324-0.7P

Fig. 12. Typical strain distributions adjacent to test weld (*two-column figure*)

6. Discussion

6.1. Provisions for Weld Design in AISC 360

In Section K5 of AISC 360-16 [4] detailed design method that considers weld effective properties (i.e., lengths and section moduli) is spelled out for plate-to-HSS and HSS-to-HSS welded joints. Therein, for the limit state of shear rupture along a plane of the weld effective throat, R_n or P_n (in connections subject to branch axial load) and $M_{n\text{-}ip}$ and $M_{n\text{-}op}$ (for connections subject to branch in-plane bending, respectively) are given as:

$$R_n \text{ or } P_n = F_{nw} t_w l_e \tag{3a}$$

$$M_{n-ip} = F_{nw} S_{ip} \tag{3b}$$

where R_n or P_n = nominal axial strength; l_e = total effective weld length of groove and fillet welds to HSS; $M_{n\text{-}ip}$ = nominal in-plane flexural strength; S_{ip} = effective elastic section modulus of welds for in-plane bending; and F_{nw} = nominal stress of the weld metal calculated in accordance with Chapter J, where:

$$F_{nw} = 0.60 F_{EXX} (1.00 + 0.5 \sin^2 \theta) \qquad \text{for fillet welds} \tag{4a}$$

$$F_{nw} = 0.60 F_{EXX} \qquad \text{for PJP groove welds} \tag{4b}$$

where θ (strictly speaking) = angle between the line of action of the required force and the weld longitudinal axis (in degrees). The parenthetical term [$(1.00+0.50\sin^{1.5}\theta)$] in Eq. (4a) is the so-called directional strength-increase factor for fillet weld(s) that applies for fillet welds connecting CHS branches to base plates, cap plates, or HSS chords [16].

According to the load and resistance factor design method of AISC 360, resistance factors of ϕ = 0.75 and 0.80 for fillet and PJP groove welds, respectively, are multiplied by Eq. (3a,b) to determine the available strength.

Previous studies have highlighted that the calculation of θ at any point along the weld axis in a CHS-to-CHS connections – let alone the value of the "sinθ factor" for the entire joint – is a complex issue. As such, it has been recommended to allow the angle θ in Eq. (4a) to be taken as the acute angle between the branch and the chord (in degrees) [16]. When $60° \leq \theta \leq 90°$, this approach yields similar results to when the "sinθ factor" is explicitly determined. Hence, a value of θ = 90° is adopted in Eq. (4a) for the fillet-welded (F-series) connections in this study.

6.2. Previous Work on Weld Design for CHS-to-CHS Connections

For axially loaded CHS-to-CHS T-, Y- and X-connections (which are within the current scope of AISC 360-22's new Table K4.2), Tousignant and Packer [15] demonstrated that the connection parameters D/t and β play a key role in determining the ratio of the effective-to-total weld length (l_e/l_w). The branch inclination angle (θ), on the other hand, does not affect the ratio l_e/l_w, but affects l_w directly.

Using experiments and FE modelling, [15] proposed the effective weld length in CHS-to-CHS T-, Y- and X-connections with $0 \leq \beta \leq 0.50$ and $60° \leq \theta \leq 90°$ be taken as Eq. (5a) (see Fig. 13):

$$l_e = \frac{4}{\sqrt{2\beta(D/t)}} l_w \leq l_w \tag{5a}$$

$$l_w = \pi D_b \frac{1+1/\sin\theta}{2} \tag{5b}$$

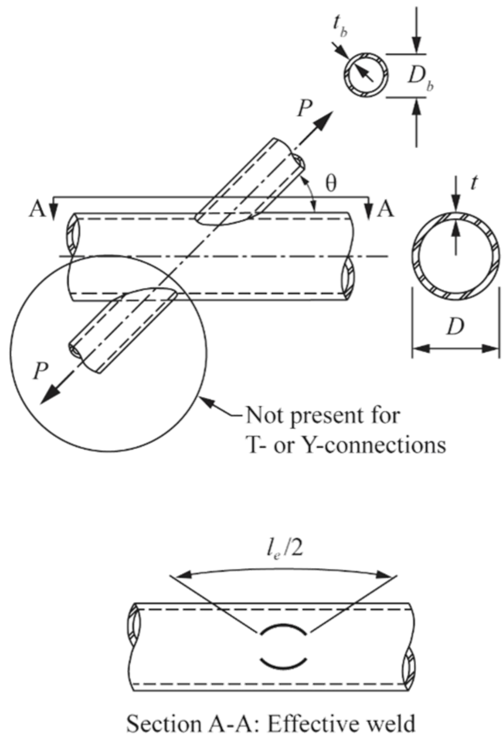

Fig. 13 Weld effective length for CHS-to-CHS T-, Y- and X-connections (*one-column figure*)

Eq. (5a), which has been adopted in AISC 360-22 Table K5.2 [23], approximates l_w by considering "branch-angle distortion" (i.e., the transformation of a circular weld into an ellipse caused by a change in θ) but ignoring "beta-ratio distortion" (which causes the plane of the elliptical weld to further distort into a saddle shape). In that regard, Eq. (5a) is conservative for connections with high β-ratios [13].

6.3. Proposal

Considering the experimental behaviour of both the fillet- and PJP-groove-welded connections demonstrated herein, for CHS-to-CHS moment T-connections subject to in-plane bending, the effective elastic section modulus can be approximated by:

$$S_{ip} = t_w \left(\frac{3 + 1/\sin\theta}{4\sin\theta} \right) \left(\frac{D_b}{2} \right)^2 \tag{6}$$

Eq. (6) is in accord with Section 9.5.4 of AWS D1.1-20 [27], which considers the weld “as a line” and – like Eq. (5b) – takes into account the branch-angle distortion but ignores beta-ratio distortion.

For CHS-to-CHS connections with small β-ratios, Eq. (6) implies that the weld is fully effective, which agrees with the previous findings of [15] and [16]. As β increases, the inherent conservatism of Eq. (6) that results from beta-ratio distortion serves as a good approximation to the ratio of the weld effective section modus to the weld gross section modulus. A consistent expression for the effective elastic section modulus of welds for out-of-plane bending S_{op} is thus [27]:

$$S_{op} = t_w \left(\frac{1 + 3/\sin\theta}{4} \right) \left(\frac{D_b}{2} \right)^2 \tag{7}$$

7. Evaluation of Proposal

7.1. Actual-to-Predicted Strength Statistics

Fig. 14a,b compares the actual strengths (M_a) of the F- and P-series CHS-to-CHS moment T-connections with the predicted nominal strengths under in-plane bending (M_{n-ip}) according to AISC 360 [Eq. (3b)], with S_{ip} from Eq. (6). It is important to note that the M_{n-ip} values in Figs. 14a,b have been calculated by using the measured values of t_w (MT, in Table 4), D_b (in Table 2), and F_{EXX} (= 592 MPa, per Table 3). In Figs. 14a,b, as well as in Table 6, tests have been grouped according to weld type/series (F- or P-) to aid in the discussion that follows.

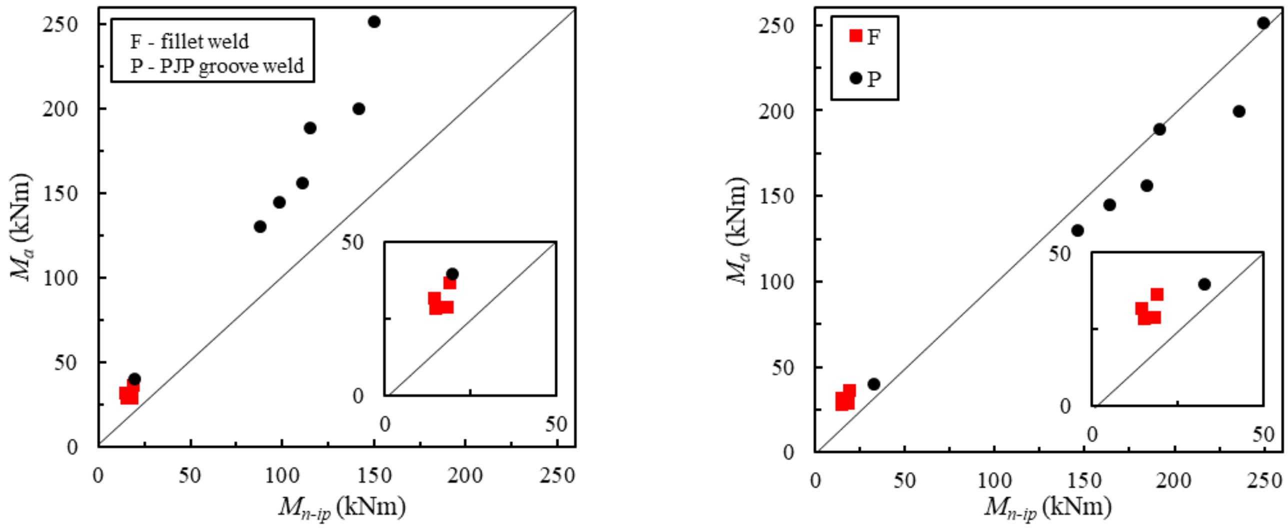

(a) Approach 1 (b) Approach 2

Fig. 14. Comparison of actual strengths and predicted strengths (*two-column figure*)

Table 6. Actual strengths, predicted strengths, and load ratios (one-*column table*)

Specimen ID	M_a kNm	Approach 1 $M_{n\text{-}ip}$ kNm	Approach 1 $M_a/M_{n\text{-}ip}$	Approach 2 $M_{n\text{-}ip}$ kNm	Approach 2 $M_a/M_{n\text{-}ip}$
T324-127-1F	36.5	19.1	1.91	19.1	1.91
T356-127-1F	28.3	15.0	1.89	15.0	1.89
T406-127-1F	28.7	18.1	1.58	18.1	1.58
T406-127-0.7F	31.6	14.5	2.19	14.5	2.19
T273-127-1P	39.8	19.7	2.02	32.8	1.21
T356-273-1P	155.9	110.8	1.41	184.7	0.84
T356-324-1P	199.8	141.6	1.41	236.0	0.85
T406-273-1P	130.0	87.9	1.48	146.4	0.89
T406-324-1P	189.0	115.2	1.64	191.9	0.98
T406-273-0.7P	145.0	98.4	1.47	164.1	0.88
T406-324-0.7P	251.6	150.0	1.68	249.9	1.01

For the F-series connections, the mean value of $M_a/M_{n\text{-}ip}$ (= δ_P) is 1.89, with a corresponding COV of 0.13. The high bias factor (δ_P) for the F-series connections is not surprising, since previous research on fillet-welded RHS-to-RHS moment T-connections [20] has shown that a direct bearing mechanism of load transfer can exist between the branch and the chord on the compression side. This, in turn, can increases S_{ip}. However, it should not be relied upon for design.

For G-series connections, the mean values of M_a/M_n (= δ_P) is 1.59, with a corresponding COV of 0.14, when F_{nw} is calculated in accordance with Eq. (4b) (i.e., as $0.60F_{EXX}$). This is termed Approach 1. However, unlike fillet welds – where the 0.6 factor in the F_{nw} equation implies that the failure mode is by shear rupture on the effective throat – the 0.6 factor in Eq. (4b) (for PJP-groove welds) is an arbitrary reduction that has been in effect since the early 1960s – to compensate for the "notch effect" of the unfused area of the joint. Because a CP detail was provided for the P-series joints (to eliminate Z-loss), it is proposed that $F_{nw} = 1.00F_{EXX}$ is more suitable for analysis. Fig. 14b shows that replacing Eq. (4b) with $F_{nw} = 1.00F_{EXX}$ for the calculation of $M_{n\text{-}ip}$ (termed Approach 2) gives $\delta_P = 0.95$ (which is closer to unity) and $V_P = 0.14$. Hence, omitting the 0.6 factor for P-series tests (Approach 2) is indeed more accurate.

When all 11 connections are considered together, $\delta_P = 1.70$ with $V_P = 0.16$ for Approach 1 (Fig. 14a), and $\delta_P = 1.29$ with $V_P = 0.39$ for Approach 2 (Fig. 14b).

7.2. Reliability Analysis using FORM

To determine the ranges of β^+ inherent in the forgoing approach(es), an approximate first-order reliability method (FORM) analysis was performed using Eq. (8) [31,32]:

$$\beta^+ = \frac{1}{\sqrt{V_R^2 + V_S^2}} \ln\left[\frac{\delta_R}{\phi}\left(\frac{\alpha_D + \alpha_L\left(L/D\right)}{\delta_D + \delta_L\left(L/D\right)}\right)\right] \tag{8}$$

where δ_R = bias coefficient for the resistance; V_R = COV of δ_R; α_D and α_L = load factors for dead and live loads, respectively (= 1.2 and 1.6, per ASCE [33]); δ_D and δ_L = bias coefficients for dead and live loads, respectively; and V_S = COV of the total load effect, taken as [34]:

$$V_S = \frac{\sqrt{\left(\delta_D V_D\right)^2 + \left(\delta_L V_L\left(L/D\right)\right)^2}}{\delta_D + \delta_L\left(L/D\right)} \tag{9}$$

where V_D and V_L = COV of the live and dead load, respectively.

Eqs. (8) and (9) incorporate the effects of live and dead load through the non-dimensional live-to-dead load ratio, L/D, which is taken to range from $1 \le L/D \le 3$ for components in steel buildings [32, 35].

7.2.1. Resistance Model and Statistical Parameters

The bias coefficient, δ_R, and the corresponding COV, V_R, are derived by assuming that the resistance is a multiplicative of four independent, lognormally distributed random variables with a bias coefficient given by [21,32]:

$$\delta_R = \delta_G \delta_M \delta_P \delta_d \tag{10}$$

and a COV that is well-approximated by:

$$V_R = \sqrt{V_G^2 + V_M^2 + V_P^2 + V_d^2} \tag{11}$$

where δ_G, δ_M, δ_P, and δ_d = bias coefficients of the geometric, material, professional, and discretization factor, respectively, and V_G, V_M, V_P and V_d = associated COVs. In the context of this paper, δ_G incorporates variability in the weld throat size; δ_M incorporates variability in electrode strength; δ_P incorporates variability in the accuracy of the design equation (used to calculate $M_{n\text{-}ip}$); and δ_d incorporates the effect of specifying discreet/commonly used weld sizes that are generally more than the minimum load and resistance factor design (LRFD) requirement.

Bias coefficients and COVs for dead and live load used in this work were taken as δ_D = 1.05, δ_L= 0.78, V_D = 0.10, and V_L = 0.32 [32], with a target of β^+ = 4.0, for connection design, in accordance with Chapter B of the AISC 360-16 Commentary [4]. Resistance factors of ϕ = 0.75 and 0.80 were adopted for fillet-welded and PJP-groove-welded T-connections connections, respectively (except as noted in Section 7.2.2).

The parameters δ_M and V_M were taken as 1.12 and 0.077, respectively, based on a large database of 672 tests performed on all-weld-metal TCs [36], and the parameters δ_G and V_G were taken as 1.03 and 0.10, respectively, to reflect common “fabrication errors” that result in variability of weld geometry [37].

The bias coefficient for the discretization factor, δ_d = 1.09, and the associated COV, V_d = 0.062, were adopted from the work of Thomas and Tousignant [38]. Although their work applied to fillet welds, an analogous approach applied to PJP-groove welds by the Authors yielded similar results.

A key finding from the current study is that the professional factor parameters (δ_P and V_P) largely depend on weld type, professional bias coefficients and their associated COVs have been calculated for fillet-welded and PJP-groove-welded joints separately, as well as together, as shown in Table 7.

Table 7. Summary of resistance parameters (*one-column table*)

	Approach 1				Approach 2			
Series	δ_P	V_P	δ_R	V_R	δ_P	V_P	δ_R	V_R
F	1.89	0.13	2.38	0.19	1.89	0.13	2.38	0.19
P	1.59	0.14	2.00	0.20	1.59	0.14	1.19	0.20
All	1.70	0.16	2.14	0.21	1.29	0.39	1.62	0.42

In the following section, inherent β^+ values are tabulated using the FORM approach (over the range of $1 \le L/D \le 3$) and compared to the target value of $\beta^+ = 4.0$, for connections, per Chapter B of the AISC 360-16 Commentary [4].

7.2.2. FORM Analysis Results

Table 8 shows the inherent β^+ values for the current tests using $\phi = 0.75$ for fillet welds, $\phi = 0.80$ for PJP-groove welds, and $\phi = 0.80$ (conservatively) for "all" welds (i.e., when all 11 tests are considered together).

Table 8. Summary of ϕ and β^+ values from the FORM approach for $1 \le L/D \le 3$ (*two-column table*)

	Range of β^+ for target ϕ		Range of ϕ for target $\beta^+ = 4.0$	
Series	Approach 1	Approach 2	Approach 1	Approach 2
F ($\phi = 0.75$)	5.87 – 6.52	5.87 – 6.52	1.30 – 1.38	1.30 – 1.38
P ($\phi = 0.80$)	4.98 – 5.42	3.26 – 3.34	1.07 – 1.14	0.64 – 0.68
All [1]	5.04 – 5.43	2.57 – 2.71	1.10 – 1.16	0.43 – 0.44

[1] using $\phi = 0.80$.

As shown in Table 8, for F-series specimens, β^+ ranges from 5.87 to 6.52 (when $\phi = 0.75$ and $1 \le L/D \le 3$) which exceeds the target value of $\beta^+ = 4.0$. For P-series specimens, taking $F_{nw} = 0.60F_{EXX}$ (Approach 1), β^+ ranges from 4.98 to 5.42 (when $\phi = 0.80$ and $1 \le L/D \le 3$), which exceeds the target. When all 11 connections (F-series and P-series) are considered together, β^+ ranges from 5.04 to 5.43.

When F_{nw} is taken as $1.00F_{EXX}$ for PJP-groove welds (Approach 2), β^+ ranges from 3.26 to 3.34 for the P-series specimens (when $\phi = 0.80$ and $1 \le L/D \le 3$) and 2.57 to 2.71 when all specimens are considered together. Results for the F-series specimens are unchanged. It is thus important to note that the 0.60 factor for F_{nw} – while being less accurate – is required for PJP-groove welds to achieve the target reliability index.

The proposal to use Eq. (6) for S_{ip} in conjunction with AISC 360-22 Chapter K [Eq. (3b)] can hence be deemed suitable if Eq. (4b) (Approach 1) is used to calculate F_{nw} for PJP-groove welds.

Figs. 15a,c show the inherent reliability indices (i.e., the results from Table 8) graphically. Therein, the discontinuities at low values of L/D are due to the intersection of the two factored load combinations from the ASCE 7 [33] [i.e., 1.4D (dead load only) and 1.2D + 1.6L].

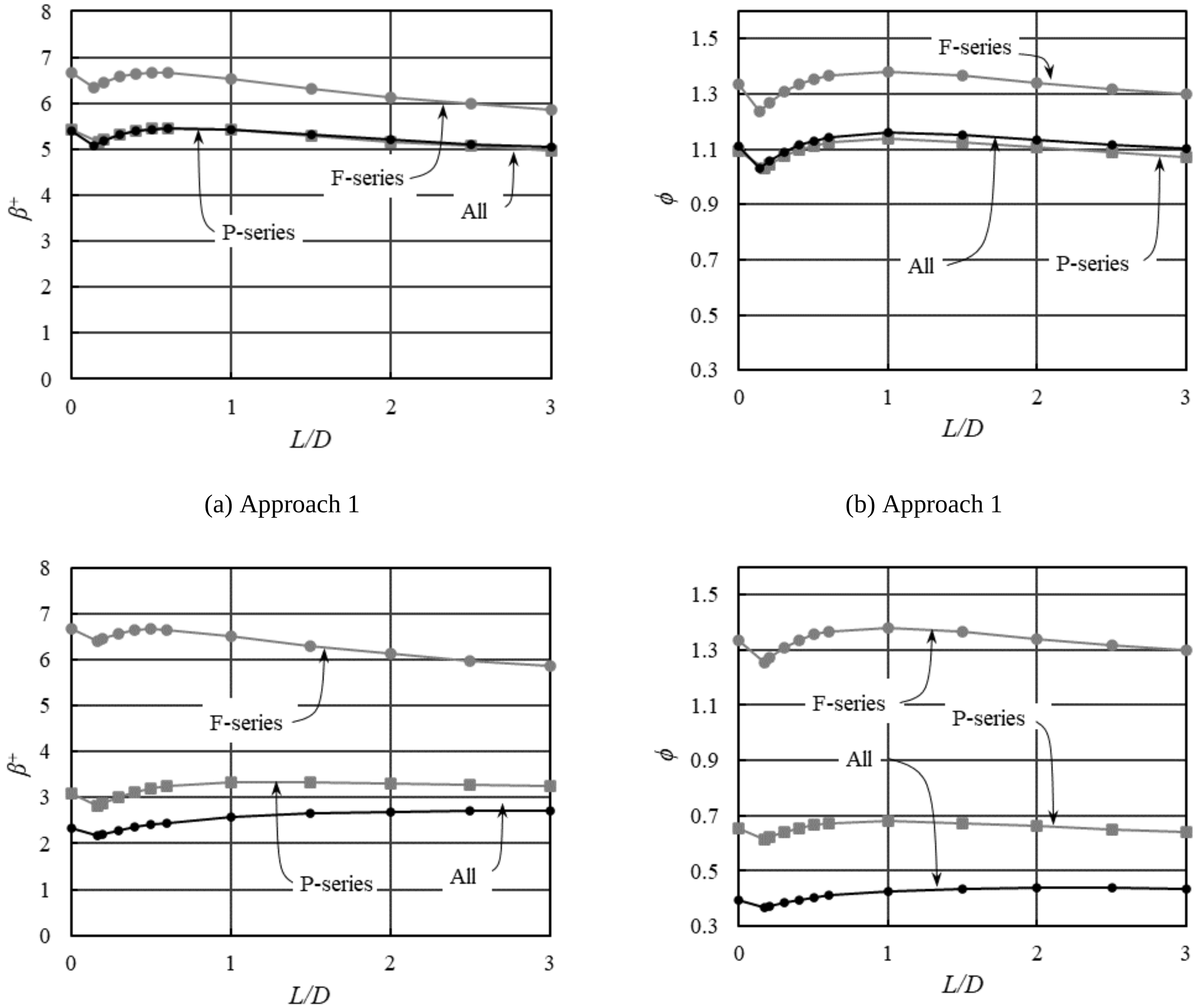

(a) Approach 1

(b) Approach 1

(c) Approach 2

(d) Approach 2

Fig. 15. β^{+} (for target ϕ) and ϕ (for target β^{+} = 4.0) vs. L/D (*two-column figure*)

Eq. (8) can also be rearranged to solve for the value(s) of ϕ required to meet/exceed the target β^{+} = 4.0. These results are also summarized in Table 8 and Figs 15b,d.

7.3. Reliability Analysis using ESF

It is interesting to compare the above results from the FORM analysis to another largely utilized reliability analysis procedure termed the “expanded separation factor” (or ESF) approach. In doing so, β^{+} and ϕ values were also calculated according to Eq. (12), which considers the statistical variation of the resistance independently of the load effects [21, 39]:

$$\beta^{+} = -\ln\left(\frac{\phi}{\phi_{\beta^{+}}\delta_{R}}\right)(\alpha_{R}V_{R})^{-1} \tag{12}$$

where $\phi_{\beta+}$ = recursive adjustment factor = $0.0062(\beta^{+})^{2} - 0.131\beta^{+} + 1.338$, and α_R = coefficient of separation, taken as 0.55. The results (which are discreet values of β^{+} and ϕ, rather than ranges) are shown in Table 9.

Table 9. Summary of ϕ and β^{+} values from the ESF approach (*two-column table*)

	β^{+} for target ϕ		ϕ for target β^{+} = 4.0	
Series	Approach 1	Approach 2	Approach 1	Approach 2
F (ϕ = 0.75)	7.58	7.58	1.42	1.42
P (ϕ = 0.80)	6.04	3.37	1.18	0.70
All [1]	6.13	3.07	1.22	0.60

[1] using ϕ = 0.80.

7.4. ESF Analysis Results

Table 9 shows that the ESF method with the $\phi_{\beta+}$ factor yields less conservative results than the FORM approach. However, it can again be concluded, based on these results, that the proposal to use Eq. (6) for S_{ip} in conjunction with AISC 360-22 Chapter K to compute the in-plane bending resistance of welds in CHS-to-CHS moment T-connections is sufficiently reliable.

8. Conclusions

From 11 tests conducted on fillet and PJP-groove welds in CHS-to-CHS moment T-connections (F- and P-series connections, respectively), evaluations of strain gauge data, comparisons of actual-to-predicted strength, and reliability analyses done according to two approaches (FORM and ESF), the following can be concluded:

- Welds in CHS-to-CHS moment T-connections are only partially effective, in theory; i.e, the maximum strain/stress does not occur at the crown point, in tension and compression.
- The design of fillet welds in CHS-to-CHS moment T-connections subjected to branch in-plane bending as "fit-for-purpose" can be carried out by using Eq. (6) for S_{ip} in conjunction with the requirements of AISC 360-16 (or -22) Section K5 [4].

- In doing so, the 0.60 factor for F_{nw} in Eq. (4b) is required for PJP-groove welds to achieve the target reliability index (even if a particular joint detail suggests otherwise).

It is therefore recommended that Eq. (6) be adopted in the new AISC 360-22 Table K5.2 for design of welds in CHS-to-CHS moment T-connections. The nonuniformity of loading will be prevalent in other types of CHS-to-CHS connections with similar geometries (i.e., Y- and X-connections) under branch in-plane bending, and hence this recommendation would also apply to those additional joints, regardless of weld type (fillet, PJP or CP), provided that the welds do not significantly change the footprint of the branch(es).

Acknowledgements

The authors gratefully acknowledge financial support from the Natural Sciences and Engineering and Research Council of Canada (NSERC). Further thanks are extended to Atlas Tube, for donating the circular hollow section (CHS) material used in this research, and to Cherubini Metal Works, for fabrication of the test specimens. The laboratory technicians in the Department of Civil and Resource Engineering at Dalhousie University (Mr. Jordan Maerz, Mr. Jesse Keane and Mr. Dean Grijm) are also gratefully acknowledged.

Notation

D	overall diameter of CHS chord
D_b	overall diameter of CHS branch
E	Young's modulus
F_{EXX}	electrode ultimate strength
F_{nw}	nominal strength of the weld metal per unit area
F_u	ultimate stress of the HSS
F_y	yield stress
L/D	live-to-dead load ratio
M_a	(applied) maximum in-plane bending moment

$M_{n\text{-}ip}$ nominal flexural strength for in-plane bending

P_a (applied) maximum force

P_n nominal axial resistance

R_n nominal resistance

S_{ip} effective elastic section modulus of weld for in-plane bending

S_{op} effective elastic section modulus of weld for out-of-plane bending

V_D coefficient of variation for dead load effect

V_G coefficient of variation for geometry

V_L coefficient of variation for live load effect

V_M coefficient of variation for material

V_P coefficient of variation for the professional factor

V_R coefficient of variation for the resistance

V_S coefficient of variation for the total load effect

d greatest perpendicular dimension measured from the branch surface to the weld surface

d_b depth of bevel

l length of chord

l_b length of branch

l_h horizontal weld leg size (in contact with the chord)

l_v vertical weld leg size (in contact with the branch)

l_e weld effective length

l_w total weld length

t wall thickness of CHS chord

t_b wall thickness of CHS branch

t_w weld effective throat dimension

α_D load factor for dead load

α_L load factor for live load

α_R coefficient of separation, taken as 0.55

β branch-to-chord width ratio

β^+ reliability index

Δ_D branch indentation

$\Delta_{flexual}$ flexural deflection of CHS branch

Δ_{rigid} rigid body deflection of CHS branch

Δ_{total} total deflection of CHS branch

δ_D bias coefficient for dead load

δ_d bias coefficient for discretization

δ_G bias coefficient for the geometry

δ_L bias coefficient for live load

δ_M bias coefficient for the material factor

δ_P bias coefficient for the professional factor

δ_R bias coefficient for the resistance

ε_{rup} rupture strain

ε_u ultimate strain

ε_y yield strain

θ angle of loading measured from the weld longitudinal axis; branch inclination angle

τ branch-to-chord thickness ratio

ϕ resistance factor

$\phi_{\beta+}$ adjustment factor = $0.0062(\beta^+)2 - 0.131\beta^+ + 1.338$

Ψ local dihedral angle

ρ subtended angle

References

[1] Wardenier, J. 1982. Hollow section joints. Delft, The Netherlands: Delft University Press.

[2] Packer, J. A., Sherman, D. R., & Lecce, M. 2010. Hollow structural section connections. AISC Steel Design Guide No. 24. Chicago, IL: American Institute of Steel Construction.

[3] International Organization for Standardization (ISO). 2013. ISO 14346:2013 (E). Static design procedure for welded hollow section joints – Recommendations. Geneva, Switzerland: International Organization for Standardization.

[4] American Institute of Steel Construction (AISC). 2016. ANSI/AISC 360-16. Specification for structural steel buildings. Chicago, IL, USA: American Institute of Steel Construction.

[5] Canadian Standards Association (CSA). 2019. CSA S16-19. Design of steel structures. Toronto, Canada: Canadian Standards Association.

[6] Frater, G. S. & Packer, J. A. 1992. Weldment design for RHS truss connections. I: Applications. *Journal of Structural Engineering, American Society of Civil Engineers* 118(10): 2784-2803.

[7] Frater, G. S. & Packer, J. A. 1992. Weldment design for RHS truss connections. II: Experimentation. *Journal of Structural Engineering, American Society of Civil Engineers* 118(10): 2804-2820.

[8] Packer, J. A. & Cassidy, C. E. 1995. Effective weld length for HSS T, Y, and X connections. *Journal of Structural Engineering, American Society of Civil Engineers* 121(10): 1402-1408.

[9] Packer, J. A. & Sun, M. 2011. Weld design for rectangular HSS connections. *Engineering Journal, American Institute of Steel Construction* 48(1): 31-48.

[10] McFadden, M. R. & Packer, J. A. 2014. Effective weld properties for hollow structural section T-connections under branch in-plane bending. *Engineering Journal, American Institute of Steel Construction* 51(4): 247-266.

[11] Tousignant, K. & Packer, J. A. 2015. Weld effective lengths for rectangular HSS overlapped K-connections. *Engineering Journal, American Institute of Steel Construction* 52 (4): 259-282.

[12] Tousignant, K. & Packer, J. A. 2015. Investigation of weld effective length rules for RHS overlapped K-connections. In Batista, E., Vellasco, P. & Lima, L. (Eds.), *Tubular Structures XV; Proc. Intern. Symp., Rio de Janeiro 27-29 May 2015.* Rotterdam: Balkema, 357-364.

[13] Tousignant, K. & Packer, J. A. 2017. Fillet weld effective lengths in CHS X-connections. I: Experiments. *Journal of Constructional Steel Research* 138: 420-431.

[14] Tousignant, K. & Packer, J. A. 2017. Numerical investigation of fillet welds in HSS-to-rigid end-plate connection. *Journal of Structural Engineering* 142(12): 4017165.

[15] Tousignant, K., & Packer, J. 2018. Fillet weld effective lengths in CHS X-connections. II: Finite element modelling, parametric study and design. *Journal of Constructional Steel Research* 141: 77-90.

[16] Tousignant, K., & Packer, J. 2019. Weld effective lengths for round HSS cross-connections under branch axial loading. *Engineering Journal, American Institute of Steel Construction* 56(3): 173-186.

[17] Tousignant, K. & Packer, J.A. 2019. Fillet welds around circular hollow sections. *Welding in the World, IIW* 63: 421-433

[18] Tousignant, K., & Packer, J. 2020. Optimized design of fillet welds for CHS joints according to EN 1993‐1‐8. *Steel Construction* 13(1): 41-51.

[19] Tousignant, K., & Packer, J. 2020. Weld design for hollow structural section connections: Application to Canadian standards. *Canadian Journal of Civil Engineering* 47: 1128-1144.

[20] Yaghoubshahi, M., Sun, M. & Tousignant, K. 2019. Design of fillet welds in RHS-to-RHS moment T-connections under branch in-plane bending. *Journal of Constructional Steel Research* 159: 122-133.

[21] Galambos, T.V. & Ravindra, M.K., 1977. The basis for load and resistance factor design criteria of steel building structures. *Canadian Journal of Civil Engineering* 4(2): 178-189.

[22] Kennedy, D.J.L. & Aly, M.G., 1980. Limit states design of steel structures – performance factors. *Canadian Journal of Civil Engineering* 7(1): 45-77.

[23] American Institute of Steel Construction (AISC). 2021. ANSI/AISC 360-22. Specification for structural steel buildings – Public review draft dated February 5th, 2021, Chicago, IL, USA: American Institute of Steel Construction.

[24] ASTM International (ASTM) 2021. ASTM A500/A500M-21A. Standard specification for cold-formed welded and seamless carbon steel structural tubing in rounds and shapes. West Conshohocken, PA, USA: ASTM International.

[25] van der Vegte, G.J. & Makino, Y. 2010. Further research on chord length and boundary conditions of CHS T- and X-joints. *Advanced Steel Construction* 6(3): 879-890.

[26] Tousignant, K. 2019. Effect of chord length and boundary conditions on welds in CHS X-joints. in *Proceedings of the 17th International Symposium on Tubular Structures (ISTS17)* 63-70.

[27] American Welding Society (AWS). 2020. AWS D1.1/D1.1M:2020. Structural welding code – Steel, 24rd ed., Miami, FL, USA.

[28] Luyties W.H. & Post J.W. 1988 Local dihedral angle equations for tubular joints and related applications, Weld. *Welding Journal* 77 (4): 51–60.

[29] Steel Tube Institution (STI). 2021. Methods to check dimensional tolerances on hollow structural sections. Glenview, IL, USA: Steel Tube Institute.

[30] Cassidy, C. E. 1993. Effective weld length for HSS T, Y, and X connections. Master of Applied Science Thesis. Toronto, Canada: University of Toronto.

[31] Nowak, A.S. & Lind, N.C., 1979. Practical code calibration procedures. *Canadian journal of civil engineering*, 6(1), pp.112–119.

[32] Schmidt, B.J. & Bartlett, F.M., 2002. Review of resistance factor for steel: resistance distributions and resistance factor calibration. *Canadian journal of civil engineering*, 29(1), pp.109–118.

[33] American Society of Civil Engineers (ASCE), 2016. Minimum Design Loads and Associated Criteria for Buildings and Other Structures. American Society of Civil Engineers.

[34] Canadian Standards Association (CSA) 2019. CSA S6:19. Canadian highway bridge design code. Toronto, Canada: Canadian Standards Association.

[35] Ellingwood, B., Galambos. T.V., MacGregor. J.G. & Cornell. C.A. 1980. Development of a Probability Based Load Criterion for American National Standard A58. Department of Commerce, National Bureau of Standards, the University of California, USA.

[36] Lesik, D.F. & Kennedy, D.J.L., 1990. Ultimate strength of fillet welded connections loaded in plane. Canadian *journal of civil engineering*, 17(1), pp.55–67.

[37] Callele, L. J., Driver, R. G. & Grondin, G. Y. 2009. Design and behavior of multi-orientation fillet weld connections. *Engineering Journal, American Institute of Steel Construction* 2009(4): 257- 272.

[38] Thomas, J. H. & Tousignant, K. 2022. Design of single-sided fillet welds under transverse load. *Journal of Structural Engineering, American Society of Civil Engineers* (under review).

[39] Fisher, J.W., Galambos, G.L., Kulak, M.K. & Ravindra, M.K. 1978. Load and resistance factor design criteria for connectors. *Journal of the Structural Division, American Society of Civil Engineers* 104(9): 1427-1441.

Figure Captions

Fig. 1. Test specimen layout and connection nomenclature

Fig. 2. Weld details and joint nomenclature

Fig. 3. Fit-up of branch to chord after profiling and bevelling

Fig. 4. As-laid welds, before griding

Fig. 5. All-weld-metal TC test plates (dimensions in mm)

Fig. 6. Fillet weld dimensions

Fig. 7. Sample weld cross-sections (MT dimension shown)

Fig. 8. Elevation of the general test set up assembly for full-scale experiments

Fig. 9. Typical strain-gauge layout

Fig. 10. Typical weld fractures

Fig. 11. Applied moment versus chord indentation plots

Fig. 12. Typical strain distributions adjacent to test weld

Fig. 13. Weld effective length for CHS-to-CHS T-, Y- and X-connections

Fig. 14. Comparison of actual strengths and predicted strengths

Fig. 15. β^{+} (for target ϕ) and ϕ (for target β^{+} = 4.0) vs. L/D